Shape-from-Shading Derived DEMs from ShadowCam Images in Permanently Shadowed Regions at the Lunar South Pole: A First Look

Ranye Jia[1], Bo Wu[1,*], Prasun Mahanti[2]

1 Research Centre for Deep Space Explorations | Department of Land Surveying and Geo-Informatics, The Hong Kong Polytechnic University, Hung Hom, Hong Kong – bo.wu@polyu.edu.hk
2 School of Earth and Space Exploration, Arizona State University, Tempe, AZ 85287, USA

Commission III, ICWG III/II

Keywords: ShadowCam, Shape-from-shading, Permanently shadowed regions, DEM, Lunar south pole

Abstract

The lunar south pole, particularly its permanently shadowed regions (PSRs), has been the focus of future lunar exploration. The solar altitude angle at the lunar south pole is less than ~ 2°, resulting in the PSRs not being directly illuminated and the possible existence of water ice in the PSRs due to the low temperatures. High-resolution digital elevation models (DEMs) in PSRs are crucial for future exploration missions and scientific research. However, existing image datasets (e.g., LROC NAC images) cannot penetrate the PSRs. Laser altimetry (e.g., LOLA) can measure the PSRs, but the DEMs derived from LOLA suffer from noises and interpolation defects. ShadowCam is a newly deployed camera onboard the Korea Pathfinder Lunar Orbiter, with a high imaging sensitivity. ShadowCam can capture the faint secondary illumination within PSRs, revealing previously indistinguishable topographic features in persistent darkness. Based on our existing Shape-from-Shading (SfS) pipeline for generating high-resolution DEMs from monocular images, we introduce a novel SfS approach that utilizes secondary illumination and reflectance to reconstruct pixel-wise high-resolution DEMs from ShadowCam images in PSRs. The approach consists of three steps: (1) modeling the secondary illumination on the target surfaces in PSRs based on the view factor; (2) optimizing a low-resolution LOLA DEM using the secondary illumination model; (3) refining the DEM to pixel-wise resolution based on SfS using the ShadowCam images. A test area (approximately 1 km × 1 km) within the PSR in the Shackleton crater near the lunar south pole is used for experimental evaluation. The results show that the DEM generated by the proposed approach is highly consistent with the direct LOLA measurements, particularly in small-scale topographic features such as crater floors and rims that are absent from the LOLA DEM. A first look at the results indicates that the proposed approach has great potential for generating high-resolution DEMs from ShadowCam images in PSRs, which can aid future exploration missions targeting the PSRs at the lunar south pole and support related scientific research on the water ice in the PSRs.

1. Introduction

Permanently shadowed regions (PSRs) are typically found in the low-elevation areas at the lunar poles, formed due to the low angle of solar illumination caused by the Moon's low obliquity. Over extended periods, PSRs remain devoid of direct sunlight, thereby creating a unique environment with persistently low temperatures. It is hypothesized that PSRs can cold-trap volatiles, such as water-ice (Li et al., 2018), making them of significant interest for future lunar exploration missions and scientific research due to their crucial research potential.

High-resolution Digital Elevation Models (DEMs) are crucial for lunar exploration missions and scientific research (De Rosa et al., 2012; Wu et al., 2014, 2018, 2020). Lunar DEMs are typically obtained through laser altimetry (Smith et al., 2010) or stereo photogrammetry (Burns et al., 2012; Wu et al., 2014). Although laser altimetry can yield highly accurate elevation measurements, the large sample spacing often results in DEMs of low spatial resolution. Stereo photogrammetry, which requires multiple overlapping images from different perspectives, usually produces DEMs with spatial resolutions that are 3–10 times finer than those of the input images (Liu & Wu, 2020). However, capturing small-scale topographic details using photogrammetry remains a challenge.

Shape-from-Shading (SfS) is a technology that reconstructs 3D geometry (shape) based on the relationships between image intensity (shading), illumination, and viewing directions (Horn, 1990; Kirk, 1987; Wu et al., 2017). In recent years, SfS has increasingly been used for high-resolution 3D mapping of planetary bodies, such as landing sites and regions of scientific interest on the lunar surface (Grumpe et al., 2014; Wu et al., 2017; Liu & Wu, 2020), as well as the Martian surface (Beyer & Kirk, 2012; Beyer, 2017; Jiang et al., 2017; Li et al., 2021; Liu & Wu, 2023). Although SfS shows less stable solutions for 3D mapping compared to conventional methods like stereo photogrammetry, it has demonstrated the capability to capture detailed pixel-wise topographic information. Grumpe et al. (2014) and Wu et al. (2017) have shown that using a low-resolution DEM derived from laser altimetry or photogrammetry to complement SfS can notably improve the convergence of SfS algorithms and achieve promising results in terms of geometric accuracy and topographic details.

The application of conventional approaches to 3D mapping in PSRs is particularly challenging due to the topography being illuminated only by weak reflectance from nearby surfaces. The ShadowCam, onboard the Korea Pathfinder Lunar Orbiter, is a newly deployed camera with imaging sensitivity that exceeds that of the LROC NAC by more than 200 times (Robinson et al., 2023). Mahanti et al. (2022) modeled the delicate illumination within the PSRs of Shackleton Crater based on the principle of radiative energy transfer (termed the “view factor”), and their results showed high consistency with actual images acquired by the ShadowCam (Mahanti et al., 2023). This indicates that the approach effectively captures essential reflectance information in PSRs, thereby facilitating the feasibility of applying image-based methods (e.g., SfS) for 3D reconstruction within PSRs.

In this paper, we introduce a novel SfS approach for pixel-wise 3D surface reconstruction within PSRs using ShadowCam images, building on our existing SfS pipeline for generating high-resolution DEMs from monocular images (Wu et al., 2017). The proposed method requires a low-resolution DEM and a ShadowCam image, along with the corresponding ephemeris information, as inputs. We use the view factor and the SfS method to generate the secondary illumination model and to optimize the input low-resolution DEM. The developed method has been validated with real ShadowCam images taken inside Shackleton Crater. Section 2 describes the method in detail, Section 3 provides validation of the approach, and Section 4 presents a brief conclusion and discussion.

2. SfS for Pixel-wise 3D Reconstruction within PSRs using ShadowCam Images

2.1 Framework of the Approach

The proposed approach is outlined in Fig. 1. Initially, a ShadowCam image and the corresponding low-resolution DEM, such as the LOLA DEM, are provided as inputs. The ShadowCam image and the low-resolution DEM are co-registered for further processing. Illumination information for the ShadowCam image can be obtained from ephemeris data. A direct illumination image is then generated based on the Lunar-Lambert reflectance model (LL model; McEwen, 1991, 1996), using the input DEM and the illumination information. This direct illumination image represents the surface reflectance intensity under direct solar illumination and serves as a secondary illumination source within the PSR.

Subsequently, the direct illumination image and input DEM are input into the secondary illumination image reconstruction module, which reconstructs the observed intensity of the surface under secondary illumination based on the input DEM. The input DEM is then gradually optimized using the reconstructed secondary illumination and the ShadowCam image. The optimization of the DEM involves two steps: firstly, the geometry of the input DEM is pre-optimized based on the secondary illumination image, and its resolution is improved in a controlled manner. Secondly, the complex secondary illumination is simplified into a directional scenario, taking into account the local geometric relationships, to provide the essential incoming illumination direction for the SfS processing. The DEM is refined hierarchically, starting from a low resolution and progressively increasing in resolution until it matches the pixel-wise detail of the ShadowCam image. As the resolution is refined, topographical details are gradually reconstructed and integrated into the DEM.

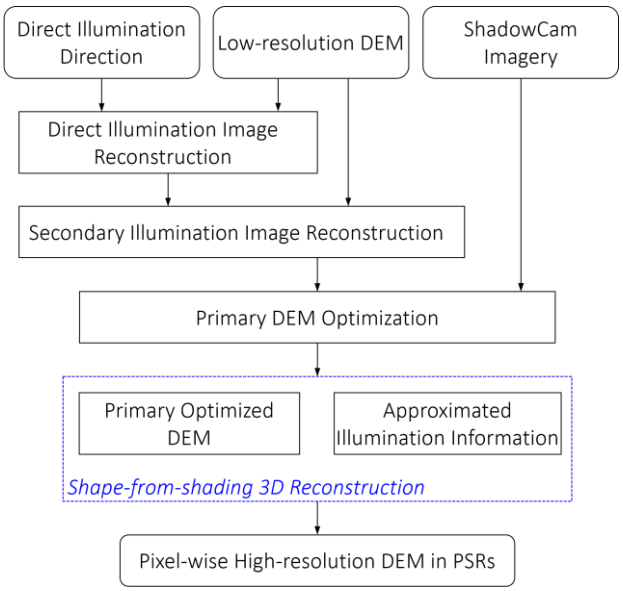

Figure 1. The framework of the proposed approach.

2.2 Reconstruction of Secondary Illumination

The 3D reconstruction of the DEM was achieved through two steps. First, the DEM initiates optimization using the secondary illumination image. Then, it is forwarded into the SfS module for pixel-wise resolution reconstruction using a ShadowCam image.

As shown in Fig. 2, the formation process of the secondary illumination model contains two components, the secondary illumination and the subsequent reflection from the illuminated interception surface.

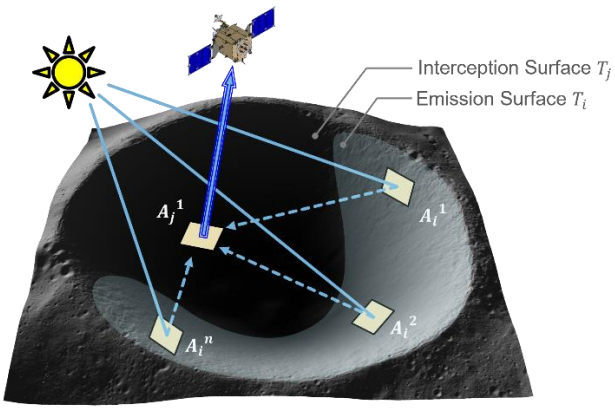

Figure 2. Conceptual illustration of secondary illumination.

We defined the reflectance intensity of secondary illumination as follows:

$$I_1(j) = R(j) \sum_{A_i \in T_i} I_0(i)\, \phi_{A_i \to A_j} \quad (1)$$

where the reflectance of secondary illumination $I_1(j)$ at each pixel j can be obtained from the cumulative result of the reflected intensities from all pixels that are under primary illumination and contribute to the observed pixel j. $I_0(i)$ represents the intensity of the reflectance from a primary illuminated pixel i, and the set T_i encompasses all such primary illuminated pixels that exert an influence on the pixel j. $\phi_{A_i \to A_j}$ denotes the attenuation coefficient, which quantifies the diminution of primary

illumination intensity as it propagates from pixel A_i to pixel A_j. Here, $\phi_{A_i \to A_j}$ serves as a scaling factor that adjusts the contribution of each primary illuminated pixel that affects the light path from A_i to A_j. We formulated $\phi_{A_i \to A_j}$ as follows:

$$\phi_{A_i \to A_j}(A_j, \theta_i, \theta_j, d) = \frac{A_j \, \theta_i \, \theta_j}{\pi d^2} \tag{2}$$

where θ_i and θ_j are the cosines of the angles between the line connecting i and j and the surface normals of i and j, respectively. v is the visibility factor, defaulting to 1, which is defined to be 0 in the absence of direct visibility. We apply the Lunar-Lambert reflectance model to define the reflectance intensity and subsequently the secondary illumination, which has been widely adopted in planetary 3D mapping. The Lunar-Lambert model is formulated with reference to the definition in (McEwen, 1991) as follows:

$$R_{LL}(\mu_0, \mu, \lambda) = (1 - \lambda)\mu_0 + 2\lambda \frac{\mu_0}{\mu_0 + \mu} \tag{3}$$

where μ_0 and μ are the cosines of the incident and emission angle relative to the surface normal, respectively. The constant parameter λ is defined by the phase angle. Defining I_1 in this form ensures that the calculated intensities are representative of the reliable physical behaviors associated with light interactions with surfaces.

2.3 Hierarchical Optimization of the DEM

The hierarchical optimization is performed in two phases: the primary DEM optimization and the pixel-wise DEM optimization. The primary DEM optimization is used to preliminarily reconstruct the geometric information of relatively larger-scale topographical features based on the input low-resolution DEM, and the pixel-wise DEM optimization is used to refine the topographical details and surface textures.

Eq. (1) represents the reflection intensity of the secondary illuminated surface based on the existing DEM, which is used to optimize the current DEM with the ShadowCam image. The existing DEM is adjusted by minimizing the residual between the ShadowCam and the reflection intensity of the secondary illuminated I_1. This primary optimization improved consistency between the input DEM and the observed topography. The optimization selectively improved the resolution, refining the details while ensuring large-scale topographical consistency. The resolution adjustments are determined such that DEM adjusted by E_0 does not introduce significant artifacts; i.e., when numerical calculations were unstable, the resolution was reduced to preserve the overall constraint from the initial DEM.

Then, we simplify the sophisticated secondary illumination into a directional illumination based on relative geometric positional relationships and perform the subsequent SfS reconstruction. The SfS module iteratively refines the DEM to achieve pixel-wise resolution. The input DEM provides the initial conditions and constrains the DEM refinement throughout the SfS process, which has been applied to lunar surface 3D reconstruction and proven effective (Wu et al., 2018). Our SfS optimizes the DEM by minimizing the following residual term:

$$E_{img} = (I_{ShadowCam} - I_{sfs})^2 \tag{4}$$

Here, $I_{ShadowCam}$ represents the intensity of the ShadowCam image, and I_{sfs} denotes the surface reflectance of the SfS-adjusted DEM. The latter is calculated using the Lunar-Lambert reflectance model referenced as Eq. (3).

The input DEM of the pixel-wise DEM optimization serves as a coarse-resolution constraint for the SfS process:

$$E_{DEM} = \left[g(Z_{ini}, \sigma) - g\left(Z_{sfs}, \sigma\right)\right]^2 \tag{5}$$

where Z_{ini} refers to the input DEM, Z_{sfs} denotes the DEM under SfS processing, and $g(*, \sigma)$ represents a Gaussian smoothing operator with σ as the pre-defined standard deviation.

The pixel-wise SfS optimization initiates from the input resolution. Each pixel is refined using the DEM and the ShadowCam image and then up-sampled to the resolution at the next pyramid level, yielding a DEM with the same resolution as that of the up-sampled data. Optimization processing continues until the resolution reaches the predefined value.

3. Experimental Analysis

The proposed approach was tested using the ShadowCam images covering the PSR inside the Shackleton crater near the lunar south pole, the corresponding LOLA DEM (20 m/pixel), and the direct LOLA measurements (https://ode.rsl.wustl.edu/moon) as ground truth for comparison. The original ShadowCam image is co-registered with the input LOLA DEM to ensure accurate alignment and integration. We extracted the test region (1.1 km × 1.1 km) at the bottom of the Shackleton crater (Fig. 3). The SfS DEM was generated using the co-registered ShadowCam image and the LOLA DEM. In the analysis, the LOLA measurements served as the validation dataset. The direct LOLA measurements are the assembled collection of discrete altimetry readings arranged along all spacecraft orbits track cross through the experiment region, offering the precise elevation of the lunar surface.

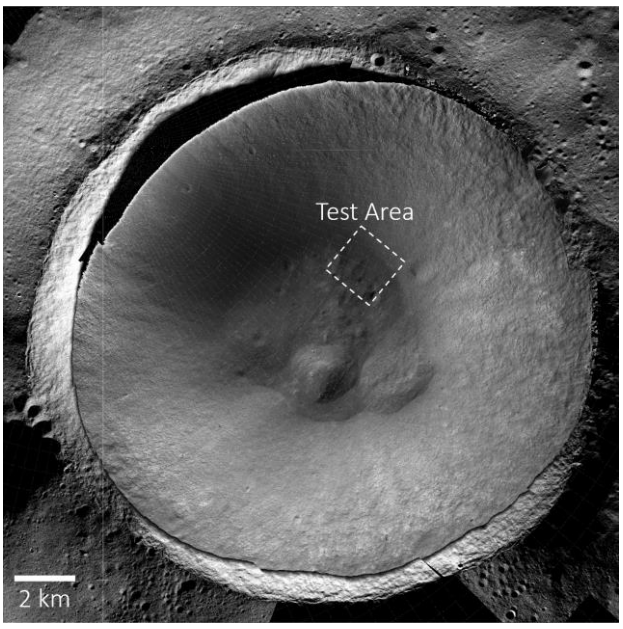

Figure 3. Testing area inside the Shackleton crater near the lunar south pole.

Fig. 4 illustrates the 3D view comparison of the input LOLA DEM (Fig. 4a) and the SfS experimental result DEM (Fig. 4b). It is apparent that the larger-scale craters at the lower of the area are clearly reconstructed. The zoomed-in display map corroborates

that the SfS DEM successfully reconstructed the small details that were not captured by the input LOLA DEM, which indicates that the SfS DEM performed higher effective spatial resolution than the LOLA DEM.

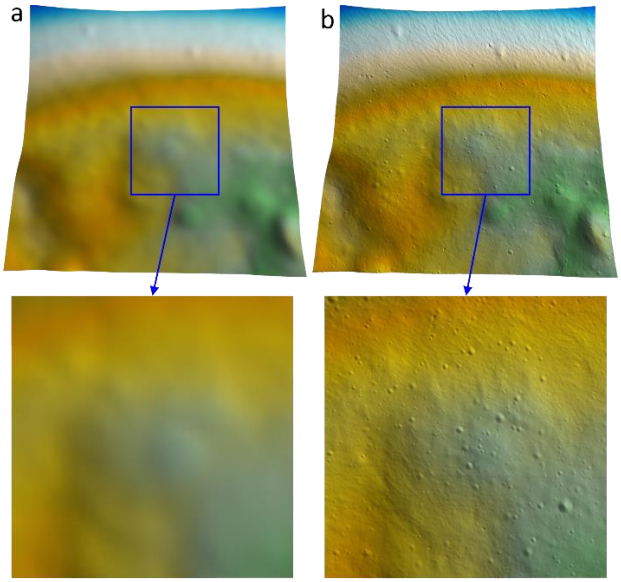

Figure 4. 3D views of (a) the input LOLA DEM (20 m/pixel), (b) the refined DEM (2 m/pixel) obtained using our approach.

Fig. 5 presents a comparison of the ShadowCam image (Fig. 5a), the shaded relief of the SfS DEM (Fig. 5b), and the shaded relief of the LOLA DEM (Fig. 5c). The SfS DEM demonstrates a spatial resolution comparable to that of the ShadowCam image, exhibiting high correspondence and effectively capturing small-scale topography details that are absent in the LOLA DEM. The zoomed view particularly highlights that the reconstructed SfS DEM fully represents the surface textures with high similarity to the ShadowCam image. This indicates that the SfS DEM revealing significant improvements in topographic detail compared to the input LOLA DEM. These enhancements underscore the effectiveness of the SfS DEM in providing a more detailed and accurate representation of the lunar surface.

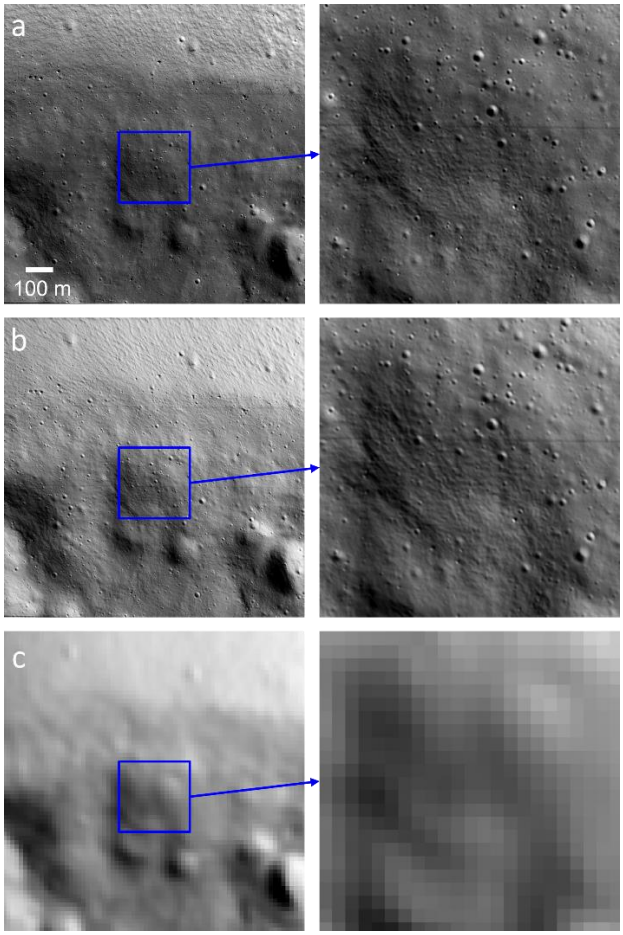

Figure 5. (a) the ShadowCam image and an enlarged view in the right column, (b) the shaded relief of the SfS DEM, and (c) the shaded relief of the input LOLA DEM for comparison.

Fig. 6 compares two topographic profiles derived from the SfS DEM, the LOLA DEM, and the direct LOLA measurements. Profile 1 traverses a relatively flat topography and intersects two small craters. The LOLA DEM profile (black dashed line) and the SfS DEM profile (blue line) exhibit high overall geometric consistency, indicating that the SfS DEM is effectively constrained by the input LOLA DEM at larger scales. The SfS DEM closely aligns with the direct LOLA measurements (red dots), providing a more refined and accurate representation of the geometric shapes of the small craters compared to the LOLA DEM. Profile 2 crosses a region characterized by significant topographic elevation relief and includes two small craters. In this area, the SfS DEM successfully reconstructs small-scale topographic features, such as the rims and floors of the craters, demonstrating full consistency with the direct LOLA measurements. In contrast, the LOLA DEM, due to its relatively lower spatial resolution, fails to capture these finer details. This comparison indicates that the SfS DEM generated by the proposed method not only reconstructs the visual shapes of the craters but also accurately represents their geometric characteristics. These results demonstrate the effectiveness of the proposed SfS approach in recovering high-resolution DEM and can improve the geometric accuracy of existing LOLA DEM, including in areas with complex topography.

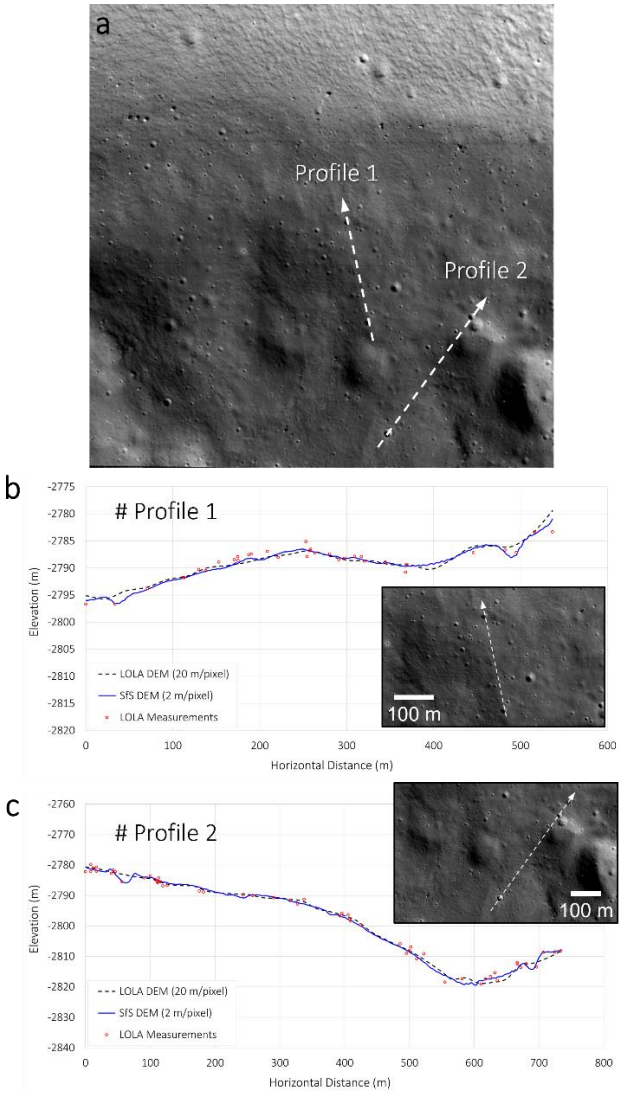

Figure 6. Profile comparison of the LOLA DEM, SfS DEM, and the direct LOLA measurements.

4. Conclusions and Discussion

This paper presents a novel SfS approach for high-resolution 3D reconstruction of the PSRs at the lunar south pole using the ShadowCam images based on the secondary illumination. The approach uses a low-resolution DEM and a co-registered ShadowCam image as inputs to generate a secondary illumination model and reconstruct a high-resolution DEM using the resulting secondary illumination information. We selected an approximately 1 km ×1 km area at the bottom of the Shackleton crater to validate our approach. The experimental results demonstrate that the DEM generated using the proposed method maintains large-scale topography consistency with the LOLA datasets and successfully captures small-scale topographic features that align with the LOLA measurements. Furthermore, the method significantly enhances the detail of the reconstructed DEM and its visual resemblance to the actual terrain. This could aid future exploration missions targeting lunar south pole PSRs and support related scientific studies of water ice in PSRs.

Notably, we simplified the complex secondary illumination into a directional illumination within the test area, considering practical reasons. This potentially leads our SfS DEM not fully to represent the topographic geometric information. Nevertheless, the proposed SfS approach exhibits encouraging performance in recovering small-scale topography features.

The proposed approach advances the application of SfS technology for 3D topographic mapping within the PSRs at the lunar south pole. In the future, our primary objective will be to more accurately model the secondary illumination within PSRs and to further refine the proposed SfS method. This will involve improving its sensitivity to complex ambient lighting conditions and enabling precise large-scale automated 3D reconstruction.

Acknowledgements

This work was supported by grants from the Research Grants Council of Hong Kong (RIF Project No: R5043-19, Project No: PolyU 15210520, Project No: 15219821). The authors would like to express thankful to the individuals who helped make the archive of the ShadowCam imagery, LOLA DEM, and related datasets publicly available.

References

Beyer, R.A., Kirk, R.L., 2012. Meter-scale slopes of candidate MSL landing sites from point photoclinometry. *Space Science Reviews*, 170, 775–791.

Beyer, R.A., 2017. Meter-scale slopes of candidate InSight landing sites from point photoclinometry. *Space Science Reviews*, 211, 97–107.

Burns, K. N., E. J. Speyerer, M. S. Robinson, T. Tran, M. R. Rosiek, B. A. Archinal, and E. Howington-Kraus, 2012. Digital Elevation Models and Derived Products from LROC NAC Stereo Observations, *International Archives of the Photogrammetry, Remote Sensing and Spatial Information Sciences*, vol. XXXIX-B4, pp. 483-488.

De Rosa, D., Bussey, B., Cahill, J.T., Lutz, T., Crawford, I.A., Hackwill, T., van Gasselt, S., Neukum, G., Witte, L., McGovern, A., Grindrod, P.M., & Carpenter, J.D., 2012. Characterisation of potential landing sites for the European Space Agency’s Lunar Lander project. *Planetary and Space Science*, 74(1), 224-246.

Grumpe, A., Belkhir, F., Wöhler, C., 2014. Construction of lunar DEMs based on reflectance modelling. *Advances in Space Research*, 53(12), 1735-1767.

Horn, B.K.P., 1990. Height and gradient from shading. *International Journal of Computer Vision*, 5(1): 37-75.

Jiang, C., Douté, S., Luo, B., et al., 2017. Fusion of photogrammetric and photoclinometric information for high-resolution DEMs from Mars in-orbit imagery. *ISPRS Journal of Photogrammetry and Remote Sensing*, 130, 418-430.

Kirk, R.L., 1987. A Fast Finite-element Algorithm for Two-dimensional Photoclinometry. Ph.D. Thesis, Caltech. pp. 165-258.

Li, S., Lucey, P. G., Milliken, R. E., Hayne, P. O., Fisher, E., Williams, J., Hurley, D. M., Elphic, R. C., 2018. Direct evidence of surface exposed water ice in the lunar polar regions, *PNAS*, 115.

Li, Z., Wu, B., Liu, W.C., Chen, Z., 2021. Integrated Photogrammetric and Photoclinometric Processing of Multiple

HRSC Images for Pixelwise 3-D Mapping on Mars. IEEE Transactions on Geoscience and Remote Sensing, 1-13.

Liu, W.C., Wu, B., 2020. An integrated photogrammetric and photoclinometric approach for illumination-invariant pixel-resolution 3D mapping of the lunar surface. *ISPRS Journal of Photogrammetry and Remote Sensing*, 159, 153–168.

Liu, W.C., Wu, B., 2023. Atmosphere-aware photoclinometry for pixel-wise 3D topographic mapping of Mars, *ISPRS Journal of Photogrammetry and Remote Sensing*, 204, 237-256

Mahanti, P., Thompson, T. J., Robinson, M. S., & Humm, D. C. 2022. View factor-based computation of secondary illumination within lunar permanently shadowed regions. *IEEE Geosci. Remote S*, 19, 1-4.

Mahanti, P., Robinson, M. S., Humm, D. C., Wagner, R. V., Estes, N. M., & Williams, J. P. 2023. Preliminary Characterization of Secondary Illumination at Shackleton Crater Permanently Shadowed Region from ShadowCam Observations and Modeling. *JASS*, 40(4), 131-148.

McEwen, A. S. (1991). Photometric functions for photoclinometry and other applications. *Icarus*, 92(2), 298-311.

Robinson, M.S., Brylow, S.M., Caplinger, M.A., Carter, L.M., Clark, M.J., Denevi, B.W., Estes, N.M., Humm, D.C., Mahanti, P., Peckham, D.A., Ravine, M.A., 2023. ShadowCam instrument and investigation overview. *JASS*. 40(4), 149-71.

Smith, D. E., Zuber, M. T., Jackson, G. B., Cavanaugh, J. F., Neumann, G. A., Riris, H., Sun, X., Zellar, R. S., Coltharp, C., Connelly, J., Katz, R. B., Kleyner, I., Liiva, P., Matuszeski, A., Mazarico, E. M., McGarry, J. F., Novo-Gradac, A.-M., Ott, M. N., Peters, C., Zagwodzki, T. W. (2010). The Lunar Orbiter Laser Altimeter Investigation on the Lunar Reconnaissance Orbiter Mission. *Space Sci. Rev.* 150(1-4), 209-241.

Wu, B., Li, F., Ye, L., Qiao, S., Huang, H., Wu, X., Zhang, H., 2014. Topographic Modeling and Analysis of the Landing Site of Chang’E-3 on the Moon. *Earth and Planetary Science Letters*, 405, 257-273.

Wu, B., Huang, J., Li, Y., Wang, Y., Peng, J., 2018. Rock Abundance and Crater Density in the Candidate Chang'E-5 Landing Region on the Moon, *Journal of Geophysical Research - Planets*, 123(12), 3256-3272.

Wu, B., Liu, W. C., Grumpe, A., Wöhler, C., 2017. Construction of pixel-level resolution DEMs from monocular images by shape and albedo from shading constrained with low-resolution DEM. *ISPRS Journal of Photogrammetry and Remote Sensing*, 140, 3-19.

Wu, B., Li, F., Hu, H., Zhao, Y., Wang, Y., Xiao, P., Li, Y., Liu, W. C., Chen, L., Ge, X., Yang, M., Xu, Y., Ye, Q., Wu, X., Zhang, H., 2020. Topographic and Geomorphological Mapping and Analysis of the Chang’E-4 Landing Site on the Far Side of the Moon, *PE&RS*, 86(4), 247-258.